Cross-section measurements of $e^+e^- \to \phi K^+ K^-$ and $e^+e^- \to \phi K_S^0 K_S^0$ at center-of-mass energies between 3.7730 GeV and 4.7008 GeV

M. Ablikim,[1] M. N. Achasov,[5,b] P. Adlarson,[75] X. C. Ai,[81] R. Aliberti,[36] A. Amoroso,[74a,74c] M. R. An,[40] Q. An,[71,58] Y. Bai,[57] O. Bakina,[37] I. Balossino,[30a] Y. Ban,[47,g] V. Batozskaya,[1,45] K. Begzsuren,[33] N. Berger,[36] M. Berlowski,[45] M. Bertani,[29a] D. Bettoni,[30a] F. Bianchi,[74a,74c] E. Bianco,[74a,74c] J. Bloms,[68] A. Bortone,[74a,74c] I. Boyko,[37] R. A. Briere,[6] A. Brueggemann,[68] H. Cai,[76] X. Cai,[1,58] A. Calcaterra,[29a] G. F. Cao,[1,63] N. Cao,[1,63] S. A. Cetin,[62a] J. F. Chang,[1,58] T. T. Chang,[77] W. L. Chang,[1,63] G. R. Che,[44] G. Chelkov,[37,a] C. Chen,[44] Chao Chen,[55] G. Chen,[1] H. S. Chen,[1,63] M. L. Chen,[1,58,63] S. J. Chen,[43] S. M. Chen,[61] T. Chen,[1,63] X. R. Chen,[32,63] X. T. Chen,[1,63] Y. B. Chen,[1,58] Y. Q. Chen,[35] Z. J. Chen,[26,h] W. S. Cheng,[74c] S. K. Choi,[11a] X. Chu,[44] G. Cibinetto,[30a] S. C. Coen,[4] F. Cossio,[74c] J. J. Cui,[50] H. L. Dai,[1,58] J. P. Dai,[79] A. Dbeyssi,[19] R. E. de Boer,[4] D. Dedovich,[37] Z. Y. Deng,[1] A. Denig,[36] I. Denysenko,[37] M. Destefanis,[74a,74c] F. De Mori,[74a,74c] B. Ding,[66,1] X. X. Ding,[47,g] Y. Ding,[41] Y. Ding,[35] J. Dong,[1,58] L. Y. Dong,[1,63] M. Y. Dong,[1,58,63] X. Dong,[76] S. X. Du,[81] Z. H. Duan,[43] P. Egorov,[37,a] Y. H. Y. Fan,[46] Y. L. Fan,[76] J. Fang,[1,58] S. S. Fang,[1,63] W. X. Fang,[1] Y. Fang,[1] R. Farinelli,[30a] L. Fava,[74b,74c] F. Feldbauer,[4] G. Felici,[29a] C. Q. Feng,[71,58] J. H. Feng,[59] K Fischer,[69] M. Fritsch,[4] C. Fritzsch,[68] C. D. Fu,[1] J. L. Fu,[63] Y. W. Fu,[1] H. Gao,[63] Y. N. Gao,[47,g] Yang Gao,[71,58] S. Garbolino,[74c] I. Garzia,[30a,30b] P. T. Ge,[76] Z. W. Ge,[43] C. Geng,[59] E. M. Gersabeck,[67] A Gilman,[69] K. Goetzen,[14] L. Gong,[41] W. X. Gong,[1,58] W. Gradl,[36] S. Gramigna,[30a,30b] M. Greco,[74a,74c] M. H. Gu,[1,58] Y. T. Gu,[16] C. Y Guan,[1,63] Z. L. Guan,[23] A. Q. Guo,[32,63] L. B. Guo,[42] M. J. Guo,[50] R. P. Guo,[49] Y. P. Guo,[13,f] A. Guskov,[37,a] T. T. Han,[50] W. Y. Han,[40] X. Q. Hao,[20] F. A. Harris,[65] K. K. He,[55] K. L. He,[1,63] F. H. H. Heinsius,[4] C. H. Heinz,[36] Y. K. Heng,[1,58,63] C. Herold,[60] T. Holtmann,[4] P. C. Hong,[13,f] G. Y. Hou,[1,63] X. T. Hou,[1,63] Y. R. Hou,[63] Z. L. Hou,[1] H. M. Hu,[1,63] J. F. Hu,[56,i] T. Hu,[1,58,63] Y. Hu,[1] G. S. Huang,[71,58] K. X. Huang,[59] L. Q. Huang,[32,63] X. T. Huang,[50] Y. P. Huang,[1] T. Hussain,[73] N Hüsken,[28,36] W. Imoehl,[28] J. Jackson,[28] S. Jaeger,[4] S. Janchiv,[33] J. H. Jeong,[11a] Q. Ji,[1] Q. P. Ji,[20] X. B. Ji,[1,63] X. L. Ji,[1,58] Y. Y. Ji,[50] X. Q. Jia,[50] Z. K. Jia,[71,58] P. C. Jiang,[47,g] S. S. Jiang,[40] T. J. Jiang,[17] X. S. Jiang,[1,58,63] Y. Jiang,[63] J. B. Jiao,[50] Z. Jiao,[24] S. Jin,[43] Y. Jin,[66] M. Q. Jing,[1,63] T. Johansson,[75] X. K.,[1] S. Kabana,[34] N. Kalantar-Nayestanaki,[64] X. L. Kang,[10] X. S. Kang,[41] R. Kappert,[64] M. Kavatsyuk,[64] B. C. Ke,[81] A. Khoukaz,[68] R. Kiuchi,[1] R. Kliemt,[14] O. B. Kolcu,[62a] B. Kopf,[4] M. Kuessner,[4] A. Kupsc,[45,75] W. Kühn,[38] J. J. Lane,[67] P. Larin,[19] A. Lavania,[27] L. Lavezzi,[74a,74c] T. T. Lei,[71,k] Z. H. Lei,[71,58] H. Leithoff,[36] M. Lellmann,[36] T. Lenz,[36] C. Li,[44] C. Li,[48] C. H. Li,[40] Cheng Li,[71,58] D. M. Li,[81] F. Li,[1,58] G. Li,[1] H. Li,[71,58] H. B. Li,[1,63] H. J. Li,[20] H. N. Li,[56,i] Hui Li,[44] J. R. Li,[61] J. S. Li,[59] J. W. Li,[50] K. L. Li,[20] Ke Li,[1] L. J Li,[1,63] L. K. Li,[1] Lei Li,[3] M. H. Li,[44] P. R. Li,[39,j,k] Q. X. Li,[50] S. X. Li,[13] T. Li,[50] W. D. Li,[1,63] W. G. Li,[1] X. H. Li,[71,58] X. L. Li,[50] Xiaoyu Li,[1,63] Y. G. Li,[47,g] Z. J. Li,[59] Z. X. Li,[16] C. Liang,[43] H. Liang,[1,63] H. Liang,[71,58] H. Liang,[35] Y. F. Liang,[54] Y. T. Liang,[32,63] G. R. Liao,[15] L. Z. Liao,[50] J. Libby,[27] A. Limphirat,[60] D. X. Lin,[32,63] T. Lin,[1] B. J. Liu,[1] B. X. Liu,[76] C. Liu,[35] C. X. Liu,[1] F. H. Liu,[53] Fang Liu,[1] Feng Liu,[7] G. M. Liu,[56,i] H. Liu,[39,j,k] H. B. Liu,[16] H. M. Liu,[1,63] Huanhuan Liu,[1] Huihui Liu,[22] J. B. Liu,[71,58] J. L. Liu,[72] J. Y. Liu,[1,63] K. Liu,[1] K. Y. Liu,[41] Ke Liu,[23] L. Liu,[71,58] L. C. Liu,[44] Lu Liu,[44] M. H. Liu,[13,f] P. L. Liu,[1] Q. Liu,[63] S. B. Liu,[71,58] T. Liu,[13,f] W. K. Liu,[44] W. M. Liu,[71,58] X. Liu,[39,j,k] Y. Liu,[39,j,k] Y. Liu,[81] Y. B. Liu,[44] Z. A. Liu,[1,58,63] Z. Q. Liu,[50] X. C. Lou,[1,58,63] F. X. Lu,[59] H. J. Lu,[24] J. G. Lu,[1,58] X. L. Lu,[1] Y. Lu,[8] Y. P. Lu,[1,58] Z. H. Lu,[1,63] C. L. Luo,[42] M. X. Luo,[80] T. Luo,[13,f] X. L. Luo,[1,58] X. R. Lyu,[63] Y. F. Lyu,[44] F. C. Ma,[41] H. L. Ma,[1] J. L. Ma,[1,63] L. L. Ma,[50] M. M. Ma,[1,63] Q. M. Ma,[1] R. Q. Ma,[1,63] R. T. Ma,[63] X. Y. Ma,[1,58] Y. Ma,[47,g] Y. M. Ma,[32] F. E. Maas,[19] M. Maggiora,[74a,74c] S. Malde,[69] Q. A. Malik,[73] A. Mangoni,[29b] Y. J. Mao,[47,g] Z. P. Mao,[1] S. Marcello,[74a,74c] Z. X. Meng,[66] J. G. Messchendorp,[14,64] G. Mezzadri,[30a] H. Miao,[1,63] T. J. Min,[43] R. E. Mitchell,[28] X. H. Mo,[1,58,63] N. Yu. Muchnoi,[5,b] J. Muskalla,[36] Y. Nefedov,[37] F. Nerling,[19,d] I. B. Nikolaev,[5,b] Z. Ning,[1,58] S. Nisar,[12,l] Y. Niu,[50] S. L. Olsen,[63] Q. Ouyang,[1,58,63] S. Pacetti,[29b,29c] X. Pan,[55] Y. Pan,[57] A. Pathak,[35] P. Patteri,[29a] Y. P. Pei,[71,58] M. Pelizaeus,[4] H. P. Peng,[71,58] K. Peters,[14,d] J. L. Ping,[42] R. G. Ping,[1,63] S. Plura,[36] S. Pogodin,[37] V. Prasad,[34] F. Z. Qi,[1] H. Qi,[71,58] H. R. Qi,[61] M. Qi,[43] T. Y. Qi,[13,f] S. Qian,[1,58] W. B. Qian,[63] C. F. Qiao,[63] J. J. Qin,[72] L. Q. Qin,[15] X. P. Qin,[13,f] X. S. Qin,[50] Z. H. Qin,[1,58] J. F. Qiu,[1] S. Q. Qu,[61] C. F. Redmer,[36] K. J. Ren,[40] A. Rivetti,[74c] V. Rodin,[64] M. Rolo,[74c] G. Rong,[1,63] Ch. Rosner,[19] S. N. Ruan,[44] N. Salone,[45] A. Sarantsev,[37,c] Y. Schelhaas,[36] K. Schoenning,[75] M. Scodeggio,[30a,30b] K. Y. Shan,[13,f] W. Shan,[25] X. Y. Shan,[71,58] J. F. Shangguan,[55] L. G. Shao,[1,63] M. Shao,[71,58] C. P. Shen,[13,f] H. F. Shen,[1,63] W. H. Shen,[63] X. Y. Shen,[1,63] B. A. Shi,[63] H. C. Shi,[71,58] J. L. Shi,[13] J. Y. Shi,[1] Q. Q. Shi,[55] R. S. Shi,[1,63] X. Shi,[1,58] J. J. Song,[20] T. Z. Song,[59] W. M. Song,[35,1] Y. J. Song,[13] Y. X. Song,[47,g] S. Sosio,[74a,74c] S. Spataro,[74a,74c] F. Stieler,[36] Y. J. Su,[63] G. B. Sun,[76] G. X. Sun,[1] H. Sun,[63] H. K. Sun,[1] J. F. Sun,[20] K. Sun,[61] L. Sun,[76] S. S. Sun,[1,63] T. Sun,[1,63] W. Y. Sun,[35] Y. Sun,[10] Y. J. Sun,[71,58] Y. Z. Sun,[1] Z. T. Sun,[50] Y. X. Tan,[71,58] C. J. Tang,[54] G. Y. Tang,[1] J. Tang,[59] Y. A. Tang,[76] L. Y Tao,[72] Q. T. Tao,[26,h] M. Tat,[69] J. X. Teng,[71,58] V. Thoren,[75] W. H. Tian,[52] W. H. Tian,[59] Y. Tian,[32,63] Z. F. Tian,[76] I. Uman,[62b] S. J. Wang,[50] B. Wang,[1] B. L. Wang,[63] Bo Wang,[71,58] C. W. Wang,[43] D. Y. Wang,[47,g] F. Wang,[72] H. J. Wang,[39,j,k] H. P. Wang,[1,63] J. P. Wang,[50] K. Wang,[1,58] L. L. Wang,[1] M. Wang,[50] Meng Wang,[1,63] S. Wang,[13,f]

S. Wang,[39,j,k] T. Wang,[13,f] T. J. Wang,[44] W. Wang,[59] W. Wang,[72] W. P. Wang,[71,58] X. Wang,[47,g] X. F. Wang,[39,j,k] X. J. Wang,[40] X. L. Wang,[13,f] Y. Wang,[61] Y. D. Wang,[46] Y. F. Wang,[1,58,63] Y. H. Wang,[48] Y. N. Wang,[46] Y. Q. Wang,[1] Yaqian Wang,[18,1] Yi Wang,[61] Z. Wang,[1,58] Z. L. Wang,[72] Z. Y. Wang,[1,63] Ziyi Wang,[63] D. Wei,[70] D. H. Wei,[15] F. Weidner,[68] S. P. Wen,[1] C. W. Wenzel,[4] U. Wiedner,[4] G. Wilkinson,[69] M. Wolke,[75] L. Wollenberg,[4] C. Wu,[40] J. F. Wu,[1,63] L. H. Wu,[1] L. J. Wu,[1,63] X. Wu,[13,f] X. H. Wu,[35] Y. Wu,[71] Y. J. Wu,[32] Z. Wu,[1,58] L. Xia,[71,58] X. M. Xian,[40] T. Xiang,[47,g] D. Xiao,[39,j,k] G. Y. Xiao,[43] S. Y. Xiao,[1] Y. L. Xiao,[13,f] Z. J. Xiao,[42] C. Xie,[43] X. H. Xie,[47,g] Y. Xie,[50] Y. G. Xie,[1,58] Y. H. Xie,[7] Z. P. Xie,[71,58] T. Y. Xing,[1,63] C. F. Xu,[1,63] C. J. Xu,[59] G. F. Xu,[1] H. Y. Xu,[66] Q. J. Xu,[17] Q. N. Xu,[31] W. Xu,[1,63] W. L. Xu,[66] X. P. Xu,[55] Y. C. Xu,[78] Z. P. Xu,[43] Z. S. Xu,[63] F. Yan,[13,f] L. Yan,[13,f] W. B. Yan,[71,58] W. C. Yan,[81] X. Q. Yan,[1] H. J. Yang,[51,e] H. L. Yang,[35] H. X. Yang,[1] Tao Yang,[1] Y. Yang,[13,f] Y. F. Yang,[44] Y. X. Yang,[1,63] Yifan Yang,[1,63] Z. W. Yang,[39,j,k] Z. P. Yao,[50] M. Ye,[1,58] M. H. Ye,[9] J. H. Yin,[1] Z. Y. You,[59] B. X. Yu,[1,58,63] C. X. Yu,[44] G. Yu,[1,63] J. S. Yu,[26,h] T. Yu,[72] X. D. Yu,[47,g] C. Z. Yuan,[1,63] L. Yuan,[2] S. C. Yuan,[1] X. Q. Yuan,[1] Y. Yuan,[1,63] Z. Y. Yuan,[59] C. X. Yue,[40] A. A. Zafar,[73] F. R. Zeng,[50] X. Zeng,[13,f] Y. Zeng,[26,h] Y. J. Zeng,[1,63] X. Y. Zhai,[35] Y. C. Zhai,[50] Y. H. Zhan,[59] A. Q. Zhang,[1,63] B. L. Zhang,[1,63] B. X. Zhang,[1] D. H. Zhang,[44] G. Y. Zhang,[20] H. Zhang,[71] H. H. Zhang,[59] H. H. Zhang,[35] H. Q. Zhang,[1,58,63] H. Y. Zhang,[1,58] J. Zhang,[81] J. J. Zhang,[52] J. L. Zhang,[21] J. Q. Zhang,[42] J. W. Zhang,[1,58,63] J. X. Zhang,[39,j,k] J. Y. Zhang,[1] J. Z. Zhang,[1,63] Jianyu Zhang,[63] Jiawei Zhang,[1,63] L. M. Zhang,[61] L. Q. Zhang,[59] Lei Zhang,[43] P. Zhang,[1,63] Q. Y. Zhang,[40,81] Shuihan Zhang,[1,63] Shulei Zhang,[26,h] X. D. Zhang,[46] X. M. Zhang,[1] X. Y. Zhang,[50] Xuyan Zhang,[55] Y. Zhang,[69] Y. Zhang,[72] Y. T. Zhang,[81] Y. H. Zhang,[1,58] Yan Zhang,[71,58] Yao Zhang,[1] Z. H. Zhang,[1] Z. L. Zhang,[35] Z. Y. Zhang,[44] Z. Y. Zhang,[76] G. Zhao,[1] J. Zhao,[40] J. Y. Zhao,[1,63] J. Z. Zhao,[1,58] Lei Zhao,[71,58] Ling Zhao,[1] M. G. Zhao,[44] S. J. Zhao,[81] Y. B. Zhao,[1,58] Y. X. Zhao,[32,63] Z. G. Zhao,[71,58] A. Zhemchugov,[37,a] B. Zheng,[72] J. P. Zheng,[1,58] W. J. Zheng,[1,63] Y. H. Zheng,[63] B. Zhong,[42] X. Zhong,[59] H. Zhou,[50] L. P. Zhou,[1,63] X. Zhou,[76] X. K. Zhou,[7] X. R. Zhou,[71,58] X. Y. Zhou,[40] Y. Z. Zhou,[13,f] J. Zhu,[44] K. Zhu,[1] K. J. Zhu,[1,58,63] L. Zhu,[35] L. X. Zhu,[63] S. H. Zhu,[70] S. Q. Zhu,[43] T. J. Zhu,[13,f] W. J. Zhu,[13,f] Y. C. Zhu,[71,58] Z. A. Zhu,[1,63] J. H. Zou,[1] and J. Zu[71,58]

(BESIII Collaboration)

[1]*Institute of High Energy Physics, Beijing 100049, People's Republic of China*
[2]*Beihang University, Beijing 100191, People's Republic of China*
[3]*Beijing Institute of Petrochemical Technology, Beijing 102617, People's Republic of China*
[4]*Bochum Ruhr-University, D-44780 Bochum, Germany*
[5]*Budker Institute of Nuclear Physics SB RAS (BINP), Novosibirsk 630090, Russia*
[6]*Carnegie Mellon University, Pittsburgh, Pennsylvania 15213, USA*
[7]*Central China Normal University, Wuhan 430079, People's Republic of China*
[8]*Central South University, Changsha 410083, People's Republic of China*
[9]*China Center of Advanced Science and Technology, Beijing 100190, People's Republic of China*
[10]*China University of Geosciences, Wuhan 430074, People's Republic of China*
[11]*Chung-Ang University, Seoul, 06974, Republic of Korea*
[12]*COMSATS University Islamabad, Lahore Campus, Defence Road,*
Off Raiwind Road, 54000 Lahore, Pakistan
[13]*Fudan University, Shanghai 200433, People's Republic of China*
[14]*GSI Helmholtzcentre for Heavy Ion Research GmbH, D-64291 Darmstadt, Germany*
[15]*Guangxi Normal University, Guilin 541004, People's Republic of China*
[16]*Guangxi University, Nanning 530004, People's Republic of China*
[17]*Hangzhou Normal University, Hangzhou 310036, People's Republic of China*
[18]*Hebei University, Baoding 071002, People's Republic of China*
[19]*Helmholtz Institute Mainz, Staudinger Weg 18, D-55099 Mainz, Germany*
[20]*Henan Normal University, Xinxiang 453007, People's Republic of China*
[21]*Henan University, Kaifeng 475004, People's Republic of China*
[22]*Henan University of Science and Technology, Luoyang 471003, People's Republic of China*
[23]*Henan University of Technology, Zhengzhou 450001, People's Republic of China*
[24]*Huangshan College, Huangshan 245000, People's Republic of China*
[25]*Hunan Normal University, Changsha 410081, People's Republic of China*
[26]*Hunan University, Changsha 410082, People's Republic of China*
[27]*Indian Institute of Technology Madras, Chennai 600036, India*
[28]*Indiana University, Bloomington, Indiana 47405, USA*
[29a]*INFN Laboratori Nazionali di Frascati, I-00044, Frascati, Italy*

[29b]INFN Sezione di Perugia, I-06100, Perugia, Italy
[29c]University of Perugia, I-06100, Perugia, Italy
[30a]INFN Sezione di Ferrara, I-44122, Ferrara, Italy
[30b]University of Ferrara, I-44122, Ferrara, Italy
[31]Inner Mongolia University, Hohhot 010021, People's Republic of China
[32]Institute of Modern Physics, Lanzhou 730000, People's Republic of China
[33]Institute of Physics and Technology, Peace Avenue 54B, Ulaanbaatar 13330, Mongolia
[34]Instituto de Alta Investigación, Universidad de Tarapacá, Casilla 7D, Arica 1000000, Chile
[35]Jilin University, Changchun 130012, People's Republic of China
[36]Johannes Gutenberg University of Mainz, Johann-Joachim-Becher-Weg 45, D-55099 Mainz, Germany
[37]Joint Institute for Nuclear Research, 141980 Dubna, Moscow region, Russia
[38]Justus-Liebig-Universitaet Giessen, II. Physikalisches Institut,
Heinrich-Buff-Ring 16, D-35392 Giessen, Germany
[39]Lanzhou University, Lanzhou 730000, People's Republic of China
[40]Liaoning Normal University, Dalian 116029, People's Republic of China
[41]Liaoning University, Shenyang 110036, People's Republic of China
[42]Nanjing Normal University, Nanjing 210023, People's Republic of China
[43]Nanjing University, Nanjing 210093, People's Republic of China
[44]Nankai University, Tianjin 300071, People's Republic of China
[45]National Centre for Nuclear Research, Warsaw 02-093, Poland
[46]North China Electric Power University, Beijing 102206, People's Republic of China
[47]Peking University, Beijing 100871, People's Republic of China
[48]Qufu Normal University, Qufu 273165, People's Republic of China
[49]Shandong Normal University, Jinan 250014, People's Republic of China
[50]Shandong University, Jinan 250100, People's Republic of China
[51]Shanghai Jiao Tong University, Shanghai 200240, People's Republic of China
[52]Shanxi Normal University, Linfen 041004, People's Republic of China
[53]Shanxi University, Taiyuan 030006, People's Republic of China
[54]Sichuan University, Chengdu 610064, People's Republic of China
[55]Soochow University, Suzhou 215006, People's Republic of China
[56]South China Normal University, Guangzhou 510006, People's Republic of China
[57]Southeast University, Nanjing 211100, People's Republic of China
[58]State Key Laboratory of Particle Detection and Electronics,
Beijing 100049, Hefei 230026, People's Republic of China
[59]Sun Yat-Sen University, Guangzhou 510275, People's Republic of China
[60]Suranaree University of Technology, University Avenue 111, Nakhon Ratchasima 30000, Thailand
[61]Tsinghua University, Beijing 100084, People's Republic of China
[62a]Turkish Accelerator Center Particle Factory Group, Istinye University, 34010, Istanbul, Turkey
[62b]Near East University, Nicosia, North Cyprus, 99138, Mersin 10, Turkey
[63]University of Chinese Academy of Sciences, Beijing 100049, People's Republic of China
[64]University of Groningen, NL-9747 AA Groningen, The Netherlands
[65]University of Hawaii, Honolulu, Hawaii 96822, USA
[66]University of Jinan, Jinan 250022, People's Republic of China
[67]University of Manchester, Oxford Road, Manchester M13 9PL, United Kingdom
[68]University of Muenster, Wilhelm-Klemm-Strasse 9, 48149 Muenster, Germany
[69]University of Oxford, Keble Road, Oxford OX13RH, United Kingdom
[70]University of Science and Technology Liaoning, Anshan 114051, People's Republic of China
[71]University of Science and Technology of China, Hefei 230026, People's Republic of China
[72]University of South China, Hengyang 421001, People's Republic of China
[73]University of the Punjab, Lahore-54590, Pakistan
[74a]University of Turin and INFN, University of Turin, I-10125, Turin, Italy
[74b]University of Eastern Piedmont, I-15121, Alessandria, Italy
[74c]INFN, I-10125, Turin, Italy
[75]Uppsala University, Box 516, SE-75120 Uppsala, Sweden
[76]Wuhan University, Wuhan 430072, People's Republic of China
[77]Xinyang Normal University, Xinyang 464000, People's Republic of China
[78]Yantai University, Yantai 264005, People's Republic of China

^{79}*Yunnan University, Kunming 650500, People's Republic of China*
^{80}*Zhejiang University, Hangzhou 310027, People's Republic of China*
^{81}*Zhengzhou University, Zhengzhou 450001, People's Republic of China*

Based on 22.7 fb^{-1} of e^+e^- annihilation data collected at 33 different center-of-mass energies between 3.7730 and 4.7008 GeV with the BESIII detector at the BEPCII collider, Born cross sections of the two processes $e^+e^- \to \phi K^+ K^-$ and $e^+e^- \to \phi K_S^0 K_S^0$ are measured for the first time. No indication of resonant production through an intermediate vector state V is observed, and the upper limits on the product of the electronic width $\Gamma_{e^+e^-}$ and the branching fraction $\mathrm{Br}(V \to \phi K\bar{K})$ of the processes $e^+e^- \to V \to \phi K^+ K^-$ and $e^+e^- \to V \to \phi K_S^0 K_S^0$ at the 90% confidence level are obtained for a large parameter space in resonance masses and widths. For the current world average mass and width of the $\psi(4230)$ of $m = 4.2187$ GeV/c^2 and $\Gamma = 44$ MeV, we set upper limits on the $\phi K^+ K^-$ and $\phi K_S^0 K_S^0$ final states of 1.75 and 0.47 eV at the 90% confidence level, respectively.

I. INTRODUCTION

In the past several years, many exotic candidates have been discovered in the charmonium and charmoniumlike spectrum. Notable examples are the $\chi_{c1}(3872)$ discovered

^{a}Also at the Moscow Institute of Physics and Technology, Moscow 141700, Russia.
^{b}Also at the Novosibirsk State University, Novosibirsk, 630090, Russia.
^{c}Also at the NRC "Kurchatov Institute," PNPI, 188300, Gatchina, Russia.
^{d}Also at Goethe University Frankfurt, 60323 Frankfurt am Main, Germany.
^{e}Also at Key Laboratory for Particle Physics, Astrophysics and Cosmology, Ministry of Education; Shanghai Key Laboratory for Particle Physics and Cosmology; Institute of Nuclear and Particle Physics, Shanghai 200240, People's Republic of China.
^{f}Also at Key Laboratory of Nuclear Physics and Ion-beam Application (MOE) and Institute of Modern Physics, Fudan University, Shanghai 200443, People's Republic of China.
^{g}Also at State Key Laboratory of Nuclear Physics and Technology, Peking University, Beijing 100871, People's Republic of China.
^{h}Also at School of Physics and Electronics, Hunan University, Changsha 410082, China.
^{i}Also at Guangdong Provincial Key Laboratory of Nuclear Science, Institute of Quantum Matter, South China Normal University, Guangzhou 510006, China.
^{j}Also at Frontiers Science Center for Rare Isotopes, Lanzhou University, Lanzhou 730000, China.
^{k}Also at Lanzhou Center for Theoretical Physics, Lanzhou University, Lanzhou 730000, China.
^{l}Also at the Department of Mathematical Sciences, IBA, Karachi 75270, Pakistan.

by Belle [1], the charged charmoniumlike $Z_c(3900)$ discovered by BESIII [2], and the $Y(4260)$ originally observed by *BABAR* [3] as a single broad peak in the $e^+e^- \to \gamma_{\mathrm{ISR}}\pi^+\pi^- J/\psi$ process, where ISR denotes initial state radiation. BESIII later revealed that the broad $Y(4260)$ peak is asymmetric and fit it with two resonances, one [the $\psi(4230)$] with a slightly lower mass than the $Y(4260)$ and one [the $\psi(4360)$] with a higher mass [4].

The $\psi(4230)$ has been clearly observed by BESIII in prominent charmonium transitions to $\pi^+\pi^- J/\psi$ [4], $\pi^+\pi^- h_c$ [5], $\pi^+\pi^-\psi(3686)$ [6], $\omega\chi_{c0}$ [7], and $\eta J/\psi$ [8–10]. However, decays into light hadrons have not been so far observed, including $p\bar{p}\pi^0$ [11], $\phi\phi\phi$, $\phi\phi\omega$ [12], $pK_S^0\bar{n}K^-$ [13], $K_S^0 K^\pm\pi^\mp$ [14], $K_S^0 K^\pm\pi^\mp\pi^0$, $K_S^0 K^\pm\pi^\mp\eta$ [15], $2(p\bar{p})$ [16], $\phi\Lambda\bar{\Lambda}$ [17], $p\bar{p}\eta$, and $p\bar{p}\omega$ [18].

While multiple theoretical approaches have attempted to classify exotic states, e.g., as tetraquarks, hadronic molecules or hybrid charmonia, there is still no full understanding of the inner structure of, e.g., the $\psi(4230)$. Their compatibility with experimental data has recently been discussed in detail in Ref. [19]. Additional sources of information, including new decay modes of the $\psi(4230)$, are needed from experiments in order to discriminate between the different hypotheses. In Ref. [20], the $\psi(4230)$ is interpreted as a diquark antidiquark state $cs\bar{c}\bar{s}$, which would lead to decays into final states containing $s\bar{s}$. In fact, this was supported by BESIII in a spin-parity analysis of the $Z_c(3900)$ in the process $e^+e^- \to \psi(4230) \to Z_c(3900)\pi \to \pi^+\pi^- J/\psi$ [21], with one of the dominant contributions coming from $e^+e^- \to \psi(4230) \to f_0(980)J/\psi$. The $f_0(980)$ meson is known to have large $s\bar{s}$ contributions [22,23]. Assuming that the $c\bar{c}$ component of the $cs\bar{c}\bar{s}$ state annihilates while the $s\bar{s}$ survives as a meson with hidden strangeness, e.g., the ϕ, the decay $e^+e^- \to \psi(4230) \to \phi K\bar{K}$ is expected to occur. Further

analyses indicating $s\bar{s}$ components of the $\psi(4230)$ can be found in [24–26].

In this work, the measurements of the energy-dependent Born cross sections of the processes $e^+e^- \to \phi K^+K^-$ and $e^+e^- \to \phi K_S^0 K_S^0$ for data collected at 33 different center-of-mass energies between 3.7730 and 4.7008 GeV with the BESIII detector are reported. Possible resonant contributions $V \to \phi K^+K^-$ and $V \to \phi K_S^0 K_S^0$ are investigated.

II. BESIII DETECTOR AND MONTE CARLO SIMULATIONS

The BESIII detector is a magnetic spectrometer [27] located at the Beijing Electron Positron Collider (BEPCII) [28]. The cylindrical core of the BESIII detector consists of a helium-based multilayer drift chamber (MDC), a plastic scintillator time-of-flight system (TOF),

TABLE I. Summary of the Born cross sections σ_B including (asymmetric) statistical and systematic uncertainties of the processes $e^+e^- \to \phi K^+K^-$ (σ_{B_1}) and $e^+e^- \to \phi K_S^0 K_S^0$ (σ_{B_2}) at different center-of-mass energies $\sqrt{s}$, integrated luminosity L, number of observed events $N_{1,2}$, efficiency $\epsilon_{1,2}$, radiative corrections $(1+\delta_r)_{1,2}$ and the vacuum polarization correction $\frac{1}{|1-\Pi|^2}$.

$\sqrt{s}$ (GeV)	L (pb^{-1})	N_1	ϵ_1 (%)	$(1+\delta_r)_1$	N_2	ϵ_2 (%)	$(1+\delta_r)_2$	$\frac{1}{|1-\Pi|^2}$	σ_{B_1} (pb)	σ_{B_2} (pb)
3.7730	2931.8	$7329.2^{+94.6}_{-92.9}$	35.8 ± 0.2	0.8295	$360.8^{+20.9}_{-19.2}$	18.0 ± 0.1	0.8281	1.0560	$16.19^{+0.24}_{-0.23} \pm 0.73$	$3.31^{+0.19}_{-0.18} \pm 0.10$
3.8695	224.0	$452.5^{+24.1}_{-22.4}$	34.7 ± 0.2	0.8889	$27.1^{+5.9}_{-4.3}$	17.6 ± 0.1	0.8864	1.0506	$12.68^{+0.68}_{-0.63} \pm 0.61$	$3.14^{+0.69}_{-0.50} \pm 0.10$
4.0076	482.0	$825.3^{+32.5}_{-30.8}$	33.7 ± 0.2	0.9390	$56.6^{+8.2}_{-6.6}$	16.2 ± 0.2	0.9346	1.0441	$10.53^{+0.43}_{-0.41} \pm 0.47$	$3.16^{+0.46}_{-0.37} \pm 0.09$
4.1285	401.5	$590.3^{+27.4}_{-25.7}$	32.4 ± 0.2	0.9675	$34.7^{+6.6}_{-5.0}$	15.8 ± 0.1	0.9611	1.0525	$9.06^{+0.43}_{-0.41} \pm 0.38$	$2.30^{+0.44}_{-0.33} \pm 0.07$
4.1574	408.7	$633.9^{+28.4}_{-26.7}$	32.4 ± 0.2	0.9739	$27.1^{+5.9}_{-4.3}$	15.2 ± 0.1	0.9667	1.0533	$9.48^{+0.44}_{-0.41} \pm 0.39$	$1.82^{+0.40}_{-0.29} \pm 0.05$
4.1784	3189.0	$4572.5^{+74.9}_{-73.2}$	32.6 ± 0.2	0.9783	$289.6^{+18.6}_{-16.9}$	15.9 ± 0.1	0.9710	1.0541	$8.67^{+0.17}_{-0.17} \pm 0.36$	$2.37^{+0.16}_{-0.14} \pm 0.07$
4.1888	524.6	$754.9^{+30.9}_{-29.2}$	32.6 ± 0.2	0.9801	$49.9^{+7.7}_{-6.1}$	16.1 ± 0.2	0.9727	1.0558	$8.68^{+0.37}_{-0.35} \pm 0.36$	$2.44^{+0.38}_{-0.30} \pm 0.07$
4.1989	526.0	$785.2^{+31.6}_{-29.9}$	32.3 ± 0.2	0.9823	$42.3^{+7.2}_{-5.6}$	15.9 ± 0.1	0.9746	1.0564	$9.05^{+0.38}_{-0.36} \pm 0.38$	$2.09^{+0.35}_{-0.28} \pm 0.06$
4.2091	518.0	$694.2^{+29.6}_{-27.9}$	31.6 ± 0.2	0.9846	$47.1^{+7.5}_{-5.9}$	16.2 ± 0.1	0.9765	1.0568	$8.28^{+0.37}_{-0.35} \pm 0.34$	$2.31^{+0.37}_{-0.29} \pm 0.07$
4.2187	514.6	$673.6^{+29.2}_{-27.5}$	32.1 ± 0.2	0.9866	$48.0^{+7.6}_{-6.0}$	16.0 ± 0.1	0.9784	1.0563	$7.94^{+0.36}_{-0.34} \pm 0.33$	$2.39^{+0.38}_{-0.30} \pm 0.07$
4.2263	1056.4	$1390.2^{+41.6}_{-39.9}$	33.1 ± 0.2	0.9882	$79.4^{+9.5}_{-7.9}$	16.0 ± 0.1	0.9798	1.0564	$7.74^{+0.25}_{-0.24} \pm 0.32$	$1.92^{+0.23}_{-0.19} \pm 0.06$
4.2357	530.3	$715.6^{+30.1}_{-28.4}$	32.2 ± 0.2	0.9902	$51.8^{+7.8}_{-6.3}$	16.5 ± 0.2	0.9820	1.0555	$8.14^{+0.35}_{-0.34} \pm 0.34$	$2.43^{+0.37}_{-0.30} \pm 0.07$
4.2438	538.1	$659.4^{+29.4}_{-27.7}$	32.1 ± 0.2	0.9919	$35.7^{+6.7}_{-5.1}$	15.8 ± 0.1	0.9832	1.0555	$7.42^{+0.34}_{-0.32} \pm 0.31$	$1.72^{+0.32}_{-0.25} \pm 0.05$
4.2580	828.4	$978.9^{+35.4}_{-33.6}$	32.9 ± 0.2	0.9951	$69.9^{+9.0}_{-7.4}$	16.1 ± 0.1	0.9867	1.0536	$6.96^{+0.26}_{-0.25} \pm 0.29$	$2.14^{+0.28}_{-0.23} \pm 0.06$
4.2666	531.1	$697.3^{+29.7}_{-28.0}$	32.7 ± 0.2	0.9970	$33.8^{+6.5}_{-4.9}$	16.0 ± 0.1	0.9882	1.0532	$7.76^{+0.34}_{-0.32} \pm 0.32$	$1.62^{+0.31}_{-0.24} \pm 0.05$
4.2776	175.7	$241.6^{+17.5}_{-15.8}$	31.4 ± 0.2	0.9990	$13.8^{+4.5}_{-2.9}$	17.0 ± 0.2	0.9898	1.0530	$8.47^{+0.62}_{-0.56} \pm 0.36$	$1.88^{+0.61}_{-0.40} \pm 0.06$
4.2879	502.4	$577.7^{+27.2}_{-25.5}$	31.4 ± 0.2	1.0010	$37.6^{+6.8}_{-5.2}$	15.7 ± 0.1	0.9918	1.0527	$7.07^{+0.34}_{-0.32} \pm 0.30$	$1.94^{+0.35}_{-0.27} \pm 0.06$
4.3121	501.2	$583.1^{+27.5}_{-25.7}$	31.9 ± 0.2	1.0056	$35.7^{+6.7}_{-5.1}$	15.8 ± 0.1	0.9955	1.0522	$7.00^{+0.34}_{-0.32} \pm 0.30$	$1.82^{+0.34}_{-0.26} \pm 0.06$
4.3374	505.0	$556.2^{+26.5}_{-24.8}$	31.0 ± 0.2	1.0105	$25.2^{+5.7}_{-4.2}$	14.9 ± 0.1	1.0001	1.0508	$6.81^{+0.33}_{-0.31} \pm 0.29$	$1.36^{+0.31}_{-0.22} \pm 0.04$
4.3583	543.9	$604.6^{+27.6}_{-25.9}$	33.1 ± 0.2	1.0141	$45.2^{+7.4}_{-5.8}$	16.7 ± 0.2	1.0032	1.0511	$6.41^{+0.30}_{-0.28} \pm 0.27$	$2.01^{+0.33}_{-0.26} \pm 0.06$
4.3774	522.7	$593.3^{+27.5}_{-25.8}$	32.4 ± 0.2	1.0177	$41.4^{+7.1}_{-5.5}$	16.1 ± 0.1	1.0063	1.0513	$6.65^{+0.32}_{-0.30} \pm 0.28$	$1.98^{+0.34}_{-0.27} \pm 0.06$
4.3964	507.8	$530.2^{+26.1}_{-24.4}$	32.0 ± 0.2	1.0214	$33.8^{+6.5}_{-4.9}$	16.0 ± 0.1	1.0094	1.0510	$6.17^{+0.31}_{-0.29} \pm 0.26$	$1.67^{+0.32}_{-0.24} \pm 0.05$
4.4156	1043.9	$1114.1^{+37.3}_{-35.6}$	32.4 ± 0.2	1.0244	$75.6^{+9.3}_{-7.7}$	16.7 ± 0.1	1.0118	1.0524	$6.21^{+0.22}_{-0.21} \pm 0.26$	$1.72^{+0.21}_{-0.18} \pm 0.05$
4.4362	569.9	$619.2^{+28.2}_{-26.5}$	32.5 ± 0.2	1.0275	$32.8^{+6.4}_{-4.8}$	15.6 ± 0.1	1.0147	1.0537	$6.27^{+0.29}_{-0.27} \pm 0.27$	$1.47^{+0.29}_{-0.22} \pm 0.04$
4.4671	111.1	$93.4^{+11.6}_{-9.9}$	32.6 ± 0.2	1.0325	$8.1^{+3.7}_{-2.1}$	18.7 ± 0.2	1.0193	1.0548	$4.81^{+0.60}_{-0.51} \pm 0.22$	$1.55^{+0.69}_{-0.40} \pm 0.05$
4.5271	112.1	$97.8^{+11.5}_{-9.8}$	33.2 ± 0.2	1.0427	$3.4^{+2.7}_{-1.2}$	18.0 ± 0.2	1.0282	1.0545	$4.86^{+0.57}_{-0.49} \pm 0.23$	$0.66^{+0.52}_{-0.22} \pm 0.02$
4.5995	586.9	$533.4^{+26.0}_{-24.3}$	32.2 ± 0.2	1.0543	$30.0^{+6.2}_{-4.6}$	16.5 ± 0.1	1.0382	1.0546	$5.16^{+0.26}_{-0.24} \pm 0.22$	$1.20^{+0.25}_{-0.18} \pm 0.04$
4.6151	102.5	$69.3^{+9.9}_{-8.2}$	32.7 ± 0.2	1.0569	$4.3^{+2.9}_{-1.4}$	16.9 ± 0.1	1.0403	1.0545	$3.77^{+0.54}_{-0.45} \pm 0.18$	$0.97^{+0.65}_{-0.31} \pm 0.03$
4.6304	511.1	$424.3^{+23.5}_{-21.8}$	32.4 ± 0.2	1.0592	$21.4^{+5.4}_{-3.8}$	15.5 ± 0.1	1.0424	1.0544	$4.66^{+0.26}_{-0.24} \pm 0.20$	$1.04^{+0.26}_{-0.18} \pm 0.03$
4.6431	541.4	$407.0^{+23.0}_{-21.3}$	31.9 ± 0.2	1.0612	$19.5^{+5.2}_{-3.6}$	16.0 ± 0.1	1.0440	1.0544	$4.28^{+0.24}_{-0.23} \pm 0.18$	$0.87^{+0.23}_{-0.16} \pm 0.03$
4.6639	523.6	$398.5^{+22.7}_{-21.0}$	31.9 ± 0.2	1.0644	$31.9^{+6.3}_{-4.8}$	15.6 ± 0.1	1.0466	1.0544	$4.32^{+0.25}_{-0.23} \pm 0.18$	$1.50^{+0.30}_{-0.23} \pm 0.05$
4.6842	1631.7	$1295.0^{+40.5}_{-38.7}$	32.0 ± 0.2	1.0677	$61.3^{+8.5}_{-6.9}$	15.3 ± 0.1	1.0492	1.0545	$4.48^{+0.14}_{-0.14} \pm 0.19$	$0.94^{+0.13}_{-0.11} \pm 0.03$
4.7008	526.2	$389.6^{+22.7}_{-21.0}$	31.9 ± 0.2	1.0704	$22.4^{+5.5}_{-3.9}$	14.0 ± 0.1	1.0515	1.0545	$4.18^{+0.24}_{-0.23} \pm 0.18$	$1.16^{+0.28}_{-0.20} \pm 0.04$

and a CsI(Tl) electromagnetic calorimeter (EMC), which are all enclosed in a superconducting solenoidal magnet providing a 1.0 T magnetic field [29]. The solenoid is supported by an octagonal flux-return yoke with resistive plate counter muon identifier modules interleaved with steel. The acceptance for charged particles and photons is 93% over the 4π solid angle. The charged-particle momentum resolution at 1 GeV/c is 0.5%, and the dE/dx resolution is 6% for the electrons from Bhabha scattering. The EMC measures photon energies with a resolution of 2.5% (5%) at 1 GeV in the barrel (end cap) region. The time resolution of the TOF barrel part is 68 ps, while that of the end cap part is 110 ps. The end cap TOF system was upgraded in 2015 with multigap resistive plate chamber technology, providing a time resolution of 60 ps [30]. This upgrade improves the data taken at 27 of the 33 center-of-mass energy points.

A Monte Carlo (MC) simulation of the BESIII detector including a realistic representation of the electronic readout, based on Geant4 [31], is used to optimize particle selection requirements, to determine the product of detector acceptance and reconstruction efficiency, and to study and estimate possible background contributions. These simulations also account for the observed beam energy spread.

Dedicated simulations with 2.5×10^5 events per center-of-mass energy of the signal processes $e^+e^- \to \phi K^+K^-$ and $e^+e^- \to \phi K_S^0 K_S^0$ with subsequent decays $\phi \to K^+K^-$ and $K_S^0 \to \pi^+\pi^-$ are generated with the KKMC [32] generator, accounting for ISR and vacuum polarization (VP).

In addition, an inclusive MC sample simulated for a center-of-mass energy of 4.1784 GeV, corresponding to the dataset with the largest integrated luminosity (see Table I), is used to study potential background contributions. This sample includes open charm processes, ISR production of vector charmonium(-like) states and continuum $q\bar{q}$ (where q is a u, d, s quark) processes. Known decay modes are modeled with EvtGen [33] using branching fractions taken from the Particle Data Group (PDG) [34], whereas unknown processes are modeled by the LUNDCHARM model [35]. Final state radiation from charged final state particles is incorporated with the PHOTOS package [36]. The inclusive MC sample at $\sqrt{s} = 4.1784$ GeV corresponds to 40 times the luminosity for the data taken at this center-of-mass energy.

III. EVENT SELECTION

The final states $K^+K^-K^+K^-$ (for $e^+e^- \to \phi K^+K^-$ with $\phi \to K^+K^-$) and $K^+K^-\pi^+\pi^-\pi^+\pi^-$ (for $e^+e^- \to \phi K_S^0 K_S^0$ with $\phi \to K^+K^-$ and $K_S^0 \to \pi^+\pi^-$) are studied in this work. The polar angle θ of each charged kaon track detected in the MDC has to satisfy $|\cos\theta| < 0.93$, and its point of closest approach to the nominal interaction point must be within 10 cm in the beam direction and within 1 cm in the plane perpendicular to the beam direction. For the selection of the

$K^+K^-\pi^+\pi^-\pi^+\pi^-$ final state, a secondary vertex fit is performed, reconstructing two tracks of oppositely charged pions to a common vertex. It is required that the flight significance satisfy $L/\sigma_L > 2$, with flight length L of K_S^0 mesons and its uncertainty σ_L. A particle identification is performed combining the TOF and MDC information to calculate a score $P(h)$ for the particle hypotheses $h = \pi$, K, p. The particle type with the largest score is assigned to each track. In addition, a minimum score of $P(h) > 10^{-5}$ is required to suppress background.

A four-(six-)constraint kinematic fit is performed to the $K^+K^-K^+K^-$ ($K^+K^-K_S^0 K_S^0$ with $K_S^0 \to \pi^+\pi^-$) hypothesis requiring four-momentum conservation between initial and final states and two additional mass constraints for the $K_S^0 \to \pi^+\pi^-$ decays. The combination yielding the smallest χ^2 value is used for the analysis. The resulting invariant mass spectra of ϕ meson candidates (the K^+K^- pair which has the closest invariant mass to the ϕ mass) for ϕK^+K^- and $\phi K_S^0 K_S^0$ are displayed in Fig. 1 for data taken at $\sqrt{s} = 4.1784$ GeV. According to the inclusive MC sample, the main background contributions are $e^+e^- \to f_2(1270)(\to K^+K^-)K^+K^-$ and $e^+e^- \to K^+K^-K^+K^-$
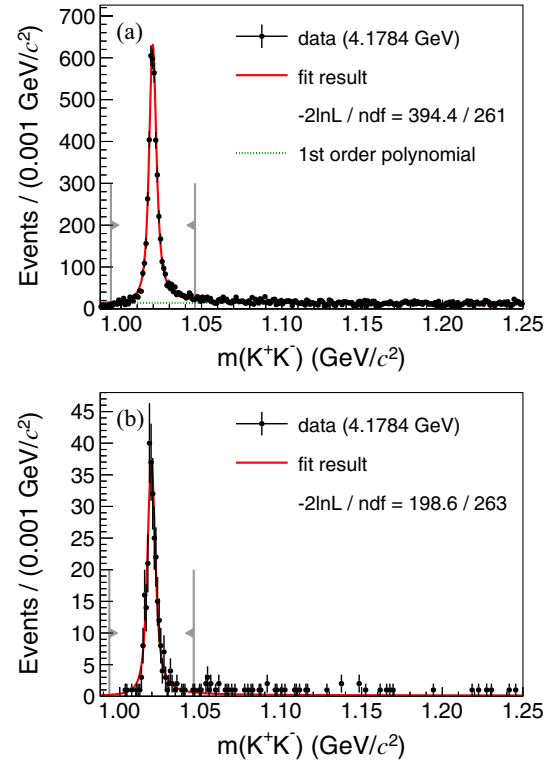

FIG. 1. Fits to the K^+K^- invariant mass distributions for the candidates of (a) $e^+e^- \to K^+K^-K^+K^-$ and (b) $e^+e^- \to K^+K^-K_S^0 K_S^0$. Black points represent data at the center-of-mass energy of 4.1784 GeV, full (red) curves represent the total fit result and, if relevant, short-dashed (green) curves show the background contribution. The gray markers indicate the signal region from which the number of observed events is obtained.

(continuum production) for the $K^+K^-K^+K^-$, and $e^+e^- \to f'_2(\to K^+K^-)K^0_S K^0_S$, $e^+e^- \to f'_2(\to K^0_S K^0_S)K^+K^-$, and $e^+e^- \to K^+K^-K^0_S K^0_S$ (continuum production) for the $K^+K^-\pi^+\pi^-\pi^+\pi^-$ final state. No peaking background is found in the K^+K^- invariant mass distribution in the vicinity of the ϕ mass.

A requirement is placed on the value of the χ^2 of the kinematic fit with N constraints, χ^2_{NC}. The threshold for this requirement is optimized according to $S/\sqrt{S+B}$, where S and B are the numbers of signal and background events in the inclusive MC sample, which have been scaled to data after applying the selection criterion. For the identification of the $K^+K^-K^+K^-$ final state, a $\chi^2_{4C} < 93$ is found as an optimal selection condition, whereas for the $K^+K^-\pi^+\pi^-\pi^+\pi^-$ final state a $\chi^2_{6C} < 227$ is chosen. Since the optimum choice in χ^2_{NC} cuts is found to be energy-independent, the requirements on the χ^2_{NC} value are applied for all center-of-mass energies. The number of signal events is determined from a fit to the invariant mass spectra (see Fig. 1). The signal part is described by a relativistic Breit-Wigner function, taking into account the asymmetric line shape of the ϕ meson due to its proximity to the K^+K^- threshold [37], convolved with a Gaussian function to account for the expected experimental mass resolution obtained from MC simulation. In the fit to events in the $K^+K^-K^+K^-$ final state, the background is described by a first-order polynomial function, while no significant increase in the fit quality has been observed when introducing a background component into the corresponding fit to the $K^+K^-\pi^+\pi^-\pi^+\pi^-$ final state. A binned maximum likelihood fit is performed to each dataset and final state individually, with the width of the ϕ meson fixed to the world average value taken from the PDG [34]. The number of signal events in final state i ($K^+K^-K^+K^-$ or $K^+K^-\pi^+\pi^-\pi^+\pi^-$) at the center-of-mass energy $\sqrt{s}$ is determined by integrating the signal function in the signal region. It is defined as the symmetric region around the nominal ϕ meson mass containing 95% of all signal events according to the signal shape. Asymmetric statistical errors due to Poisson statistics for low statistics datasets are obtained via a fit to a likelihood scan of the number of signal events. These likelihood scans are parametrized by asymmetric Gaussian distributions

$$L_i(N) = \frac{1}{\sqrt{2\pi\sigma_k^2}} \cdot e^{-\frac{(N-\mu)^2}{2\sigma_k^2}},$$

$$\text{with} \quad \sigma_k = \begin{cases} \sigma_L, & N \le \mu \\ \sigma_R, & N > \mu \end{cases}, \tag{1}$$

μ being the number of observed signal events in the maximum likelihood case and σ_L and σ_R being the lower and upper statistical uncertainty of μ for data set i, respectively. Results are listed in Table I.

IV. EFFICIENCY DETERMINATION

The efficiency $\epsilon^i(s)$ in final state i for a center-of-mass energy $\sqrt{s}$ is defined according to

$$\epsilon^i(s) = \frac{N^i_{acc}(s)}{N^i_{gen}(s)}, \tag{2}$$

with $N^i_{acc}(s)$ being the number of reconstructed signal events and $N^i_{gen}(s)$ being the total size of the signal MC sample. Equation (2) only provides a good representation of the efficiency if the signal MC sample properly reflects data in all relevant coordinates $\vec{x} = \{p_\phi, \theta_\phi, \varphi_\phi, p_K, \theta_K, \varphi_K, \ldots\}$, with p_i, θ_i, and φ_i being the momentum, polar angle and azimuthal angle, respectively. Since the data distribution is not constant over the full n-particle phase space and, in fact, is *a priori* unknown, a partial wave analysis of the data is performed in order to reweight the MC sample.

The isobar model [38] is used in the partial wave analysis by decomposing the full $e^+e^- \to \gamma^* \to \phi K^+K^-$ and $e^+e^- \to \gamma^* \to \phi K^0_S K^0_S$ processes into a sequence of two-body decays. Each two-body decay is described in the helicity formalism [39]. The K^0_S meson is treated as a stable particle in the amplitude analysis. Signal MC simulations are employed to derive the line shape of the ϕ meson that is used for normalization in the partial wave analysis. Blatt-Weisskopf barrier factors [39] are used for both the production $\gamma^* \to a + d$ and the two-body decay $a \to b + c$ according to Ref. [40]. The final model only includes processes of the type $e^+e^- \to \phi f_J$, with $f_J \to K^+K^-$ or $f_J \to K^0_S K^0_S$. Due to limited statistics, we restrict ourselves to $J^{PC} = 0^{++}$ and $J^{PC} = 2^{++}$ quantum numbers for the f_J resonances, which leads to a sufficiently good description of the data. The dynamics of the $J^{PC} = 0^{++}$ contributions are described by a K-matrix approach up to $m(K\bar{K}) \le$ 1.9 GeV, incorporating the five channels $\pi\pi$, $K\bar{K}$, $\eta\eta$, $\eta\eta'$, and 4π with the five fixed poles $f_0(980)$, $f_0(1300)$, $f_0(1500)$, and $f_0(1750)$ [41]. An additional $J^{PC} = 0^{++}$ resonance is included for respective states at higher invariant masses, while the $J^{PC} = 2^{++}$ contributions are described by four resonances. These single resonances are parametrized as relativistic Breit-Wigner amplitudes and their masses and widths are free parameters in the fit. This is justified by the fact that the aim of this partial wave analysis is only to better describe the data so as to enable an accurate determination of the efficiency. In further model tests, no significant contribution of $e^+e^- \to KK^*$ with $K^* \to \phi K$ is found.

The partial wave analysis is performed as an unbinned maximum likelihood fit using the software package PAWIAN [42]. Details on the likelihood construction in PAWIAN can be found in Refs. [40,42,43]. The few remaining background events underneath the ϕ peak ($|m_{\phi,PDG} - m(K^+K^-)| < 0.01$ GeV/c^2) are neglected in
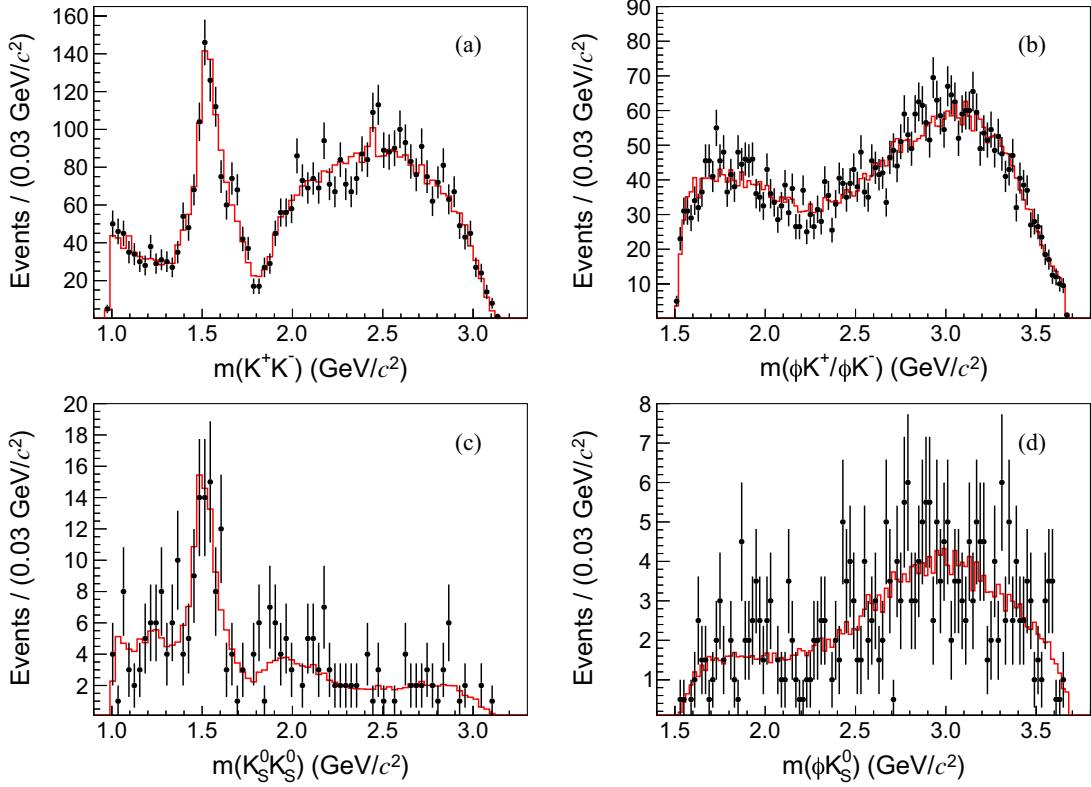
FIG. 2. Results of the partial wave analysis of the (a),(b) $e^+e^- \rightarrow \phi K^+ K^-$ and (c),(d) $e^+e^- \rightarrow \phi K_S^0 K_S^0$ processes for the data taken at a center-of-mass energy of 4.1784 GeV. The left column shows the invariant mass of the $K^+ K^-$ ($K_S^0 K_S^0$) system recoiling off the ϕ meson, the right column the invariant mass of the $\phi K^+/\phi K^-$ (ϕK_S^0) system. Black points correspond to data and full (red) curves show the result of the amplitude analysis. Note: For the $e^+e^- \rightarrow \phi K_S^0 K_S^0$ process, the solution of the fit to data from all energy points is applied to data at this center-of-mass energy as an example.

the partial wave analysis. Due to the limited statistics, the data for the $K^+K^-\pi^+\pi^-\pi^+\pi^-$ final state are fitted simultaneously over the whole energy range with all amplitudes fully constrained between the datasets apart from an overall scaling factor. The results of the partial wave analysis for the different final states are displayed in Fig. 2 for the high statistics data taken at a center-of-mass energy of 4.1784 GeV. For each energy point, we obtain event weights, $w(\vec{x})$, from the partial wave analysis as a function of the coordinates in the n-particle phase space. The efficiency $\epsilon^i(s)$ is then determined as

$$\epsilon^i(s) = \frac{\sum_{j=0}^{N_{\text{acc}}^i(s)} w(\vec{x}_j)}{\sum_{j=0}^{N_{\text{gen}}^i(s)} w(\vec{x}_j)}. \qquad (3)$$

The efficiencies obtained in this way are summarized in Table I.

V. DETERMINATION OF BORN CROSS SECTIONS

The Born cross sections of the processes $e^+e^- \rightarrow \phi K^+ K^-$ and $e^+e^- \rightarrow \phi K_S^0 K_S^0$ are determined by

$$\sigma_B(s) = \frac{N(s)}{L(s) \cdot (1 + \delta_r(s)) \cdot \frac{1}{|1-\Pi|^2} \cdot \epsilon(s) \cdot Br}, \qquad (4)$$

with $N(s)$ denoting the number of signal events observed in the data at the center-of-mass energy $\sqrt{s}$, $L(s)$ being the corresponding integrated luminosity determined using Bhabha scattering [44], $\delta_r(s)$ and $\frac{1}{|1-\Pi|^2}$ being corrections accounting for ISR and VP, $\epsilon(s)$ being the efficiency and Br corresponding to the product of branching ratios involved in the decay [$Br = Br(\phi \rightarrow K^+ K^-)$ for $e^+e^- \rightarrow \phi K^+ K^-$ and $Br = Br(\phi \rightarrow K^+ K^-) \times Br(K_S^0 \rightarrow \pi^+\pi^-)^2$ for $e^+e^- \rightarrow \phi K_S^0 K_S^0$]. The correction $\frac{1}{|1-\Pi|^2}$ is calculated with the alphaQED software package [45] with an accuracy of 0.5%. The ISR effect is treated in an iterative procedure starting from a flat energy dependence of the Born cross section $\sigma_B(s)$. It depends on the shape of the cross section and can, in general, have an effect on the efficiency. The procedure is considered converged once two successive iterations i and $i-1$ give $\kappa_i/\kappa_{i-1} = 1$ within statistical uncertainties, where $\kappa(s) = \epsilon(s) \cdot (1 + \delta_r(s))$ is the product of the efficiency and the corresponding radiative correction factor $1 + \delta_r(s)$ obtained from the KKMC MC
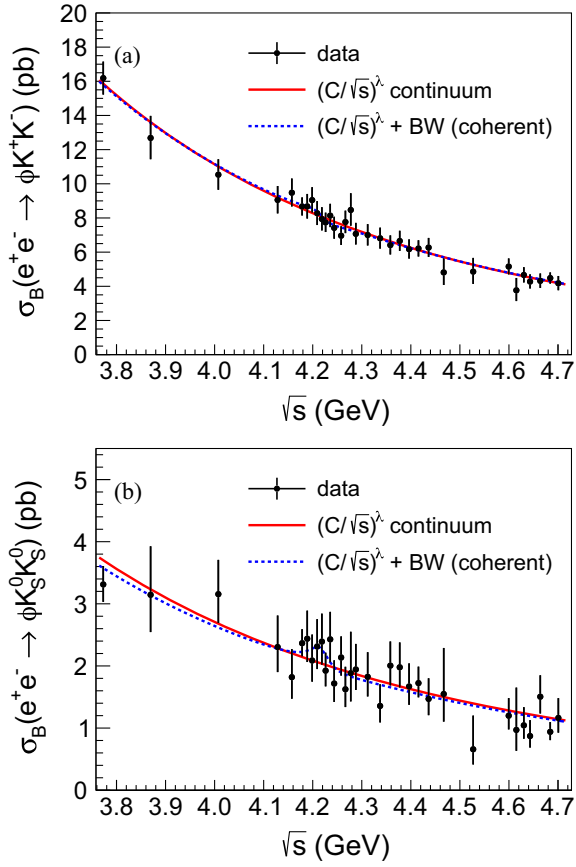
FIG. 3. Born cross sections of the (a) $e^+e^- \to \phi K^+K^-$ and (b) $e^+e^- \to \phi K^0_S K^0_S$ processes as a function of the center-of-mass energy. Black points represent our results including both statistical and systematic uncertainties. The full (red) and dashed (blue) curves represent the fits using a continuum contribution [with $C = (5.95 \pm 0.09)$ GeV pb$^{-1/\lambda}$, $\lambda = 6.06 \pm 0.28$ for $e^+e^- \to \phi K^+K^-$ and $C = (4.82 \pm 0.06)$ GeV pb$^{-\lambda}$, $\lambda = 5.35 \pm 0.47$ for $e^+e^- \to \phi K^0_S K^0_S$] and a Breit-Wigner coherently added to the continuum contribution, respectively. The fits displayed ($m = 4.2187$ GeV/c^2 and $\Gamma = 44$ MeV) are those for the current world average parameters of the $\psi(4230)$ [34].

For multiple final state charged particles per event, the corresponding uncertainties of each track are added linearly. Uncertainties on the quoted branching fractions are taken from the PDG [34].

Additional uncertainties due to selection conditions are investigated by varying each selection condition around its default value. The resulting Born cross section is determined and compared with the nominal value using the ratio $R = \frac{\sigma_{\text{step}}}{\sigma_{\text{nom}}}$. The systematic uncertainty is estimated as a standard deviation of a weighted sample of R. Here, $1/\delta R$ is used as the weight, where δR is the uncertainty taking the sizeable correlation between the event samples into account. With regard to the kinematic fit, where a selection condition of $\chi^2 < 93$ ($\chi^2 < 227$) is applied in case of the $K^+K^-K^+K^-$ ($K^+K^-\pi^+\pi^-\pi^+\pi^-$) final state, the selection condition is varied between $\chi^2 < 43$ ($\chi^2 < 177$) and $\chi^2 < 143$ ($\chi^2 < 277$) in steps of $\delta\chi^2 = 5$. For the background description, the polynomial shapes are increased by one and two orders from the nominal first-order polynomial used to fit the K^+K^- invariant mass spectrum in case of the $K^+K^-K^+K^-$ final state. For the ISR correction factor, we perform two additional iterations and found no significant difference and therefore neglected it as a source for systematic uncertainty. The uncertainty associated with the K^0_S reconstruction is determined based on studies of the control samples $J/\psi \to K^*(892)^{\mp}K^{\pm}$ and $J/\psi \to \phi K^0_S K^{\mp}\pi^{\pm}$ [48]. The nominal symmetric signal region containing 95% of the total signal is altered to a set of both smaller and larger signal regions. No systematic effect is observed here. To estimate a systematic uncertainty arising from the choice of the partial wave analysis (PWA) model, an additional $J^{PC} = 0^{++}$ as well as $J^{PC} = 2^{++}$ resonance is added. The deviation in the efficiency and hence Born cross section is used as the systematic uncertainty. Its value of 1% is found to be energy independent. The systematic uncertainties are summarized in Table II for the data taken at a center-of-mass energy of 4.1784 GeV.

generator for each iteration [46]. The resulting Born cross sections are shown in Fig. 3. Table I summarizes the Born cross sections together with the relevant values that are used for the calculation. In the case of continuum production of the two final states, a value of two is expected for the quotient of the Born cross section if isospin conservation holds.

VI. SYSTEMATIC UNCERTAINTIES

The integrated luminosity has been determined using Bhabha scattering and its uncertainty is found to be 1% [44]. The systematic uncertainty of the tracking efficiency has been determined using a $J/\psi \to p\bar{p}\pi^+\pi^-$ control sample [47] and estimated to be 1% per track.

TABLE II. Summary of relative systematic uncertainties of the Born cross section measurement in percent for the data at $\sqrt{s} = 4.1784$ GeV.

	$K^+K^-K^+K^-$	$K^+K^-\pi^+\pi^-\pi^+\pi^-$
Luminosity	1.0	1.0
Tracking efficiency	4.0	2.0
Branching fraction	1.0	1.0
χ^2 cut	0.1	0.2
Background description	0.4	
K^0_S reconstruction		2.0
PWA model	1.0	1.0
Total	4.4	3.3
Range over all energies	*4.3–5.0*	*3.2–3.4*

The total systematic uncertainty is obtained by adding each contribution in quadrature. The systematic uncertainties are obtained for various datasets individually.

VII. SEARCH FOR RESONANT CONTRIBUTIONS

In order to search for possible $e^+e^- \to V \to \phi K^+ K^-$ ($e^+e^- \to V \to \phi K^0_S K^0_S$) resonant contributions, two different fits are performed. In the first fit, only a nonresonant contribution of the type [11]

$$\sigma_{\mathrm{nr}}(s) = \left(\frac{C}{\sqrt{s}}\right)^\lambda \tag{5}$$

is used. The second fit includes a single Breit-Wigner amplitude of the form [49]

$$A_{\mathrm{res}}(s) = \frac{\sqrt{12\pi\Gamma_{e^+e^-}\mathrm{Br}(V \to \phi K\bar{K})\Gamma}}{s - m^2 + im\Gamma}, \tag{6}$$

with $\hbar^2 c^2/\mathrm{GeV}^2 = 0.3894$ mb that is coherently added to the nonresonant term, where m and Γ denote the mass and width of the resonance, respectively. The product $\zeta_V = \Gamma_{e^+e^-}\mathrm{Br}(V \to \phi K\bar{K})$ of the electronic width $\Gamma_{e^+e^-}$ and the branching fraction $\mathrm{Br}(V \to \phi K\bar{K})$ of the resonance V is a free parameter in the fit and is associated with the amplitude's strength. Maximum likelihood fits are performed where the likelihood $L(x;\Theta)$ with the given data x and the fit parameters Θ is defined as the product $L(x;\Theta) = \prod_i L_i(\Theta)$, with L_i being the likelihood function for dataset i. These likelihood functions are transformed such that they only depend on the expected number of signal events $N \equiv N_i(\Theta)$ which can be calculated for each dataset according to Eq. (4). The likelihoods $L_i(N)$ obtained from data in Eq. (1) are modified to incorporate the systematic uncertainties of dataset i. In the fit, all systematic uncertainties apart from the one on the branching ratio of the meson decays are considered uncorrelated between the different center-of-mass energies. While a correlation of a systematic uncertainty between two center-of-mass energies cannot in general be ruled out, our assumption of a vanishing correlation leads to the most conservative signal estimate.

No evidence for a resonant contribution from the fits is found and the upper limit for a wide range of resonance parameters m and Γ at the 90% confidence level are set. As the resonant contribution is added coherently according to

$$\sigma_{\mathrm{coh}} = |\sqrt{\sigma_{\mathrm{nr}}(s)} + A_{\mathrm{res}}(s) \cdot e^{i\phi}|^2 \tag{7}$$

with phase ϕ, the fit finds two ambiguous solutions for constructive and destructive interference [50]. The upper limits are obtained by integrating $L(x;\Theta) = \prod_i L_i(\Theta)$ according to
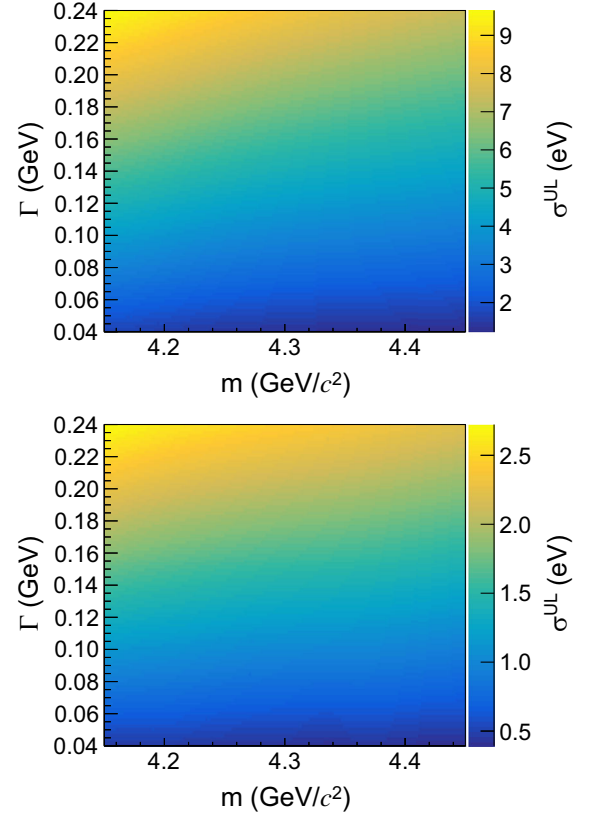

FIG. 4. Upper limits on a possible resonant contribution with mass m and width Γ added coherently to the continuum contribution for $e^+e^- \to \phi K^+ K^-$ (top) and $e^+e^- \to \phi K^0_S K^0_S$ (bottom).

$$\frac{\int_{-\infty}^{\zeta_V^{\mathrm{UL}}} L(x,\Theta)\pi(\Theta)d\zeta_V}{\int_{-\infty}^{\infty} L(x,\Theta)\pi(\Theta)d\zeta_V} = 0.90, \tag{8}$$

where the prior $\pi(\Theta)$ is given by

$$\pi(\Theta) = \begin{cases} 1, & \zeta_V \geq 0 \\ 0, & \zeta_V < 0 \end{cases}. \tag{9}$$

The procedure outlined above is repeated with a step size of 1 MeV for different masses m in the range 4.15 GeV/c^2 < m < 4.45 GeV/c^2 and widths Γ in the range 40 MeV < Γ < 240 MeV for a potential resonant contribution. The results are shown in Fig. 4. The dependence of the upper limits on the mass and widths of a resonant contribution V is observed to be flat. The upper limits for a resonant contribution of the $\psi(4230)$, using current world average values for mass ($m = 4.2187$ GeV/c^2) and width ($\Gamma = 44$ MeV) [34] are $\zeta_{V,\mathrm{coh}}^{\mathrm{UL}} = 1.75$ eV and $\zeta_{V,\mathrm{incoh}}^{\mathrm{UL}} = 0.019$ eV for $\phi K^+ K^-$ and $\zeta_{V,\mathrm{coh}}^{\mathrm{UL}} = 0.47$ eV and $\zeta_{V,\mathrm{incoh}}^{\mathrm{UL}} = 0.025$ eV for $\phi K^0_S K^0_S$ at the 90% confidence level.

VIII. SUMMARY

The processes $e^+e^- \to \phi K^+ K^-$ and $e^+e^- \to \phi K_S^0 K_S^0$ have been studied for the first time using 22.7 fb^{-1} of electron-positron annihilation data taken at 33 different center-of-mass energies between 3.7730 and 4.7008 GeV. The decay of the ϕ meson is clearly identified in both processes for all center-of-mass energies, and Born cross sections are determined with a precision of 8–20%. No evidence for a resonant contribution is found from a fit to the $e^+e^- \to \phi K^+ K^-$ and $e^+e^- \to \phi K_S^0 K_S^0$ Born cross sections. This indicates that the $\psi(4230)$ strongly prefers to preserve its charm content in decays. The upper limits at the 90% confidence level for a wide range of resonance parameters m and Γ are set.

Since the continuum contributions to the Born cross sections for both processes $e^+e^- \to \phi K^+ K^-$ and $e^+e^- \to \phi K_S^0 K_S^0$ are similar in shape, a constant fit is performed to its ratio yielding a proportionality factor of 3.85 ± 0.01. This result differs significantly from the value of two, thereby, revealing an isospin symmetry breaking effect. Since the continuum production of the final states investigated goes through a virtual photon, isospin is *a priori* not conserved.

[1] S. K. Choi *et al.* (Belle Collaboration), Phys. Rev. Lett. **91,** 262001 (2003).

[2] M. Ablikim *et al.* (BESIII Collaboration), Phys. Rev. Lett. **110,** 252001 (2013).

[3] B. Aubert *et al.* (*BABAR* Collaboration), Phys. Rev. Lett. **95,** 142001 (2005).

[4] M. Ablikim *et al.* (BESIII Collaboration), Phys. Rev. Lett. **114,** 092003 (2015); **118,** 092001 (2017).

[5] M. Ablikim *et al.* (BESIII Collaboration), Phys. Rev. Lett. **118,** 092002 (2017).

[6] M. Ablikim *et al.* (BESIII Collaboration), Phys. Rev. D **96,** 032004 (2017).

[7] M. Ablikim *et al.* (BESIII Collaboration), Phys. Rev. D **99,** 091103 (2019).

[8] M. Ablikim *et al.* (BESIII Collaboration), Phys. Rev. D **86,** 071101 (2012).

[9] M. Ablikim *et al.* (BESIII Collaboration), Phys. Rev. D **91,** 112005 (2015).

[10] M. Ablikim *et al.* (BESIII Collaboration), Phys. Rev. D **102,** 031101 (2020).

[11] M. Ablikim *et al.* (BESIII Collaboration), Phys. Lett. B **771,** 45 (2017).

[12] M. Ablikim *et al.* (BESIII Collaboration), Phys. Lett. B **774,** 78 (2017).

[13] M. Ablikim *et al.* (BESIII Collaboration), Phys. Rev. D **98,** 032014 (2018).

[14] M. Ablikim *et al.* (BESIII Collaboration), Phys. Rev. D **99,** 072005 (2019).

[15] M. Ablikim *et al.* (BESIII Collaboration), Phys. Rev. D **99,** 012003 (2019).

[16] M. Ablikim *et al.* (BESIII Collaboration), Phys. Rev. D **103,** 052003 (2021).

[17] M. Ablikim *et al.* (BESIII Collaboration), Phys. Rev. D **104**, 052006 (2021).

[18] M. Ablikim *et al.* (BESIII Collaboration), Phys. Rev. D **104**, 092008 (2021).

[19] N. Brambilla, S. Eidelman, C. Hanhart, A. Nefediev, C. P. Shen, C. E. Thomas, A. Vairo, and C. Z. Yuan, Phys. Rep. **873**, 1 (2022).

[20] L. Maiani, F. Piccinini, A. D. Polosa, and V. Riquer, Phys. Rev. D **72**, 031502 (2005).

[21] M. Ablikim *et al.* (BESIII Collaboration), Phys. Rev. Lett. **119**, 072001 (2017).

[22] R. Aaij *et al.* (LHCb Collaboration), Phys. Rev. D **89**, 092006 (2014).

[23] R. Aaij *et al.* (LHCb Collaboration), Phys. Rev. D **90**, 012003 (2014).

[24] M. Ablikim *et al.* (BESIII Collaboration), Phys. Rev. D **101**, 012008 (2020).

[25] M. Ablikim *et al.* (BESIII Collaboration), Chin. Phys. C **46**, 111002 (2022).

[26] K. Zhu, Phys. Rev. D **105**, L031506 (2022).

[27] M. Ablikim *et al.* (BESIII Collaboration), Nucl. Instrum. Methods Phys. Res., Sect. A **614**, 345 (2010).

[28] C. H. Yu *et al.*, in *Proceedings of IPAC2016, Busan, Korea* (2016), 10.18429/JACoW-IPAC2016-TUYA01.

[29] K. X. Huang *et al.*, Nucl. Sci. Tech. **33**, 142 (2022).

[30] X. Li *et al.*, Radiat. Detect. Technol. Methods **1**, 13 (2017); Y. X. Guo *et al.*, Radiat. Detect. Technol. Methods **1**, 15 (2017).

[31] S. Agostinelli *et al.* (GEANT4 Collaboration), Nucl. Instrum. Methods Phys. Res., Sect. A **506**, 250 (2003).

[32] S. Jadach, B. F. L. Ward, and Z. Was, Phys. Rev. D **63**, 113009 (2001); Comput. Phys. Commun. **130**, 260 (2000).

[33] D. J. Lange, Nucl. Instrum. Methods Phys. Res., Sect. A **462**, 152 (2001); R. G. Ping, Chin. Phys. C **32**, 599 (2008).

[34] R. L. Workman *et al.* (Particle Data Group), Prog. Theor. Exp. Phys. **2022**, 083C01 (2022).

[35] J. C. Chen, G. S. Huang, X. R. Qi, D. H. Zhang, and Y. S. Zhu, Phys. Rev. D **62**, 034003 (2000); R. L. Yang, R. G. Ping, and H. Chen, Chin. Phys. Lett. **31**, 061301 (2014).

[36] E. Richter-Was, Phys. Lett. B **303**, 163 (1993).

[37] A. Ryd *et al.*, EvtGen: A Monte Carlo generator for B-physics, Report No. EVTGEN-V00-11-07, 2005.

[38] D. Herndon, P. Soding, and R. J. Cashmore, Phys. Rev. D **11**, 3165 (1975).

[39] S. U. Chung, Phys. Rev. D **57**, 431 (1998); **48**, 1225 (1993); **56**, 4419(E) (1997); S. U. Chung and J. M. Friedrich, Phys. Rev. D **78**, 074027 (2008).

[40] M. Ablikim *et al.* (BESIII Collaboration), Phys. Rev. D **100**, 052012 (2019).

[41] V. Anisovich and A. Sarantsev, Eur. Phys. J. A **16**, 229 (2003).

[42] B. Kopf, H. Koch, J. Pychy, and U. Wiedner, Hyperfine Interact. **229**, 69 (2014).

[43] M. Albrecht *et al.* (Crystal Barrel Collaboration), Eur. Phys. J. C **80**, 453 (2020).

[44] M. Ablikim *et al.* (BESIII Collaboration), Chin. Phys. C **39**, 093001 (2015).

[45] F. Jegerlehner, Nuovo Cimento C **034S1**, 31 (2011).

[46] W. Sun, T. Liu, M. Jing, L. Wang, B. Zhong, and W. Song, Front. Phys. **16**, 64501 (2021).

[47] W. L. Yuan, X. C. Ai, X. B. Ji, S. J. Chen, Y. Zhang, L. H. Wu, L. L. Wang, and Y. Yuan, Chin. Phys. C **40**, 026201 (2016).

[48] M. Ablikim *et al.* (BESIII Collaboration), Phys. Rev. Lett. **116**, 052001 (2016).

[49] M. Ablikim *et al.* (BESIII Collaboration), Phys. Rev. D **101**, 012008 (2020).

[50] K. Zhu, X. H. Mo, C. Z. Yuan, and P. Wang, Int. J. Mod. Phys. A **26**, 4511 (2011).